Noninvasive Imaging of Atherosclerotic Lesions in Apolipoprotein E–Deficient and Low-Density-Lipoprotein Receptor–Deficient Mice with Annexin A5

Satoshi Isobe[1], Sotirios Tsimikas[2], Jun Zhou[1], Shinichiro Fujimoto[1], Masayoshi Sarai[1], Michael J. Branks[2], Ai Fujimoto[1], Leonard Hofstra[3], Chris P. Reutelingsperger[4], Toyoaki Murohara[5], Renu Virmani[6], Frank D. Kolodgie[6], Navneet Narula[7], Artiom Petrov[1], and Jagat Narula[1]

[1]Division of Cardiology, University of California, Irvine School of Medicine, Irvine, California; [2]Division of Cardiovascular Diseases, University of California, San Diego, La Jolla, California; [3]Department of Cardiology, Maastricht University Hospital, Maastricht, The Netherlands; [4]Division of Biochemistry, Maastricht University, Maastricht, The Netherlands; [5]Department of Cardiology, Nagoya University Graduate School of Medicine, Nagoya, Japan; [6]Armed Forces Institute of Pathology, Washington, District of Columbia; and [7]Department of Pathology, University of California, Irvine School of Medicine, Irvine, California

Transgenic mice such as apolipoprotein E–deficient (apoE$^{-/-}$) and low-density-lipoprotein receptor–deficient (LDLR$^{-/-}$) mice exhibit hypercholesterolemia and develop complex atherosclerotic lesions similar to those seen in humans. Radiolabeled annexin A5 has been successfully used to noninvasively image experimental and clinical atherosclerotic disease. We evaluated the feasibility of annexin A5 imaging in transgenic apoE$^{-/-}$ and LDLR$^{-/-}$ mice with or without a cholesterol diet. **Methods:** Thirty-three mice (mean age, 62 ± 0.9 wk old) were used. Of these 33 mice, apoE$^{-/-}$ mice with the cholesterol diet for 4 mo (n = 5) and without the cholesterol diet (n = 8) and LDLR$^{-/-}$ mice with the cholesterol diet for 6 mo (n = 7) and without the cholesterol diet (n = 7) were compared with 6 normal wild-type (C57BL/6) mice with the same genetic background. ^{99m}Tc-annexin A5 was injected in 31 animals for noninvasive imaging using micro-SPECT/CT. After in vivo micro-SPECT/CT, aortas were explanted to acquire ex vivo images and calculate the percentage injected dose per gram (%ID/g) annexin uptake, followed by histologic and immunohistochemical characterization. For the evaluation of precise target localization, biotinylated annexin A5 was injected in the remaining 2 normally fed apoE$^{-/-}$ mice. **Results:** Aortic lesions were clearly visualized noninvasively by micro-SPECT and aorta calcification was detectable by micro-CT. The quantitative uptake of annexin A5 was highest in the cholesterol-fed apoE$^{-/-}$ (0.88 ± 0.27 %ID/g) mice, followed by the normal chow-fed apoE$^{-/-}$ (0.60 ± 0.16 %ID/g), the cholesterol-fed LDLR$^{-/-}$ (0.59 ± 0.14 %ID/g), the chow-fed LDLR$^{-/-}$ (0.40 ± 0.31 %ID/g), and the control (0.15 ± 0.05 %ID/g) mice. The histologic extent of atherosclerosis paralleled radiotracer uptake, and immunohistochemical studies revealed a significant correlation between radiotracer uptake and both macrophage infiltration and the extent of apoptosis. Intravenously injected biotinylated annexin A5 localized in apoptotic and nonapoptotic macrophages. **Conclusion:** This study demonstrates the feasibility of noninvasive imaging of atherosclerosis with radiolabeled annexin A5 in transgenic mouse models of human atherosclerosis.

Key Words: apoE$^{-/-}$ mice; LDLR$^{-/-}$ mice; cholesterol diet; apoptosis; ^{99m}Tc-annexin A5

J Nucl Med 2006; 47:1497–1505

Apolipoprotein E–deficient (apoE$^{-/-}$) and low-density-lipoprotein receptor–deficient (LDLR$^{-/-}$) mice develop extensive atherosclerosis in the aorta and large arteries (*1–3*). Whereas both models are spontaneously hyperlipidemic and develop atherosclerotic lesions, apoE$^{-/-}$ mice generally develop more extensive hypercholesterolemia and lesion formation with a high fat/cholesterol diet than LDLR$^{-/-}$ mice (*4*). The morphology, cellular composition, and predilection sites of atherosclerotic lesions in these mice have been well documented and reflect human atherosclerosis in many aspects (*5–8*). In view of the similarities of these lesions with human disease, apoE$^{-/-}$ and LDLR$^{-/-}$ mice have been used extensively for the investigation of atherogenic mechanisms and antiatherogenic intervention studies. It is conceivable that development of a noninvasive imaging strategy will allow convenient characterization and efficacy of intervention in transgenic mice models.

Annexin A5 has been successfully used for noninvasive imaging of atherosclerotic lesions in an experimental rabbit model and preliminary studies of symptomatic carotid atherosclerosis in patients undergoing carotid endarterectomy (*9,10*). Annexin A5 is a naturally occurring protein and has a nanomolar affinity for binding to phosphatidylserine (PS),

Received Apr. 16, 2006; revision accepted Jun. 12, 2006.

For correspondence or reprints contact: Artiom Petrov, PhD, Division of Cardiology, University of California, Irvine School of Medicine, Medical Science Building I, Room C 112, Irvine, CA 92697.

E-mail: adpetrov@uci.edu

which is prominently expressed on the outer cell membrane surface of the apoptotic cells (*11,12*). Because apoptosis of macrophages contributes to the vulnerability of plaques to rupture (*9*), annexin uptake has been proposed to predict the likelihood of acute vascular events.

In the present study, we evaluated the ability of ^{99m}Tc-annexin A5 to detect the presence, prevalence, and magnitude of atherosclerotic lesions in the aorta of transgenic apoE$^{-/-}$ and LDLR$^{-/-}$ mice, to characterize the effects of a high fat/cholesterol diet on imaging parameters, and to assess whether the radiotracer uptake correlates with the presence of macrophages and apoptotic cells.

MATERIALS AND METHODS

Animal Models

Thirty-three mice were used in this study. Thirteen homozygous apoE$^{-/-}$ mice (hybrid with a C57BL/6 × 129ola background) and 14 homozygous LDLR$^{-/-}$ mice (with a C57BL/6 × 129Sv background) from colonies established from breeders provided by The Jackson Laboratory were used. Six wild-type mice (C57BL/6) with the same genetic background were also used as control animals. The mean age of all mice was 62 ± 0.9 wk old. Animals were divided into 5 groups as follows: apoE$^{-/-}$ mice fed with a normal mouse chow (n = 8); apoE$^{-/-}$ mice fed with a diet containing 0.15% cholesterol for 4 mo (n = 5); LDLR$^{-/-}$ mice fed with a normal mouse chow (n = 7); LDLR$^{-/-}$ fed mice with a diet containing 0.15% cholesterol for 6 mo (n = 7); and control mice with a normal chow (n = 6). The study protocol for imaging and tissue harvesting was approved by the institutional animal research and care committees at the University of California, Irvine, and University of California, San Diego, CA, respectively. Of the 33 animals, 31 received ^{99m}Tc-annexin A5 for noninvasive imaging of atherosclerotic lesions. In the remaining 2 apoE$^{-/-}$ mice without the cholesterol diet, biotinylated annexin A5 was administered for identification of the basis of annexin A5 uptake by direct immunohistochemical staining.

Annexin A5 and Radiolabeling

Human recombinant annexin A5, expressed in *Escherichia coli*, was derivatized with nicotinic acid analog hydrazinonicotinamide (HYNIC; Anor Med) by gentle mixing. HYNIC is a bifunctional molecule with an affinity for lysine residues of proteins on 1 moiety and for the conjugates of ^{99m}Tc on the other; the stable complex formed by this molecule did not affect protein bioreactivity (data not shown). To bind ^{99m}Tc to the HYNIC-annexin A5 conjugate, a reduced tin (stannous ion) and tricine solution (20 μL; 200 μL of 20 mmol/L tricine and 40 μg/mL $Sn{\cdot}2H_2O$) was added to ^{99m}Tc-pertechnetate (100 μL) with an aliquot of HYNIC-annexin A5 (100 μL) under anoxic conditions. The final specific radioactivity was 370–7,400 kBq/μg (10–200 μCi/μg) protein. Thin-layer chromatography showed a radiopurity of approximately 90%–98%.

In Vivo and Ex Vivo Annexin A5 Imaging Protocols

For atherosclerosis imaging targeting apoptotic cells, ^{99m}Tc-annexin A5 (175 ± 18 MBq) was injected intravenously through the dorsal tail vein and animals were anesthetized with 2.0% isoflurane for imaging procedures. For CT enhancement, a contrast agent (0.4 mL, Fenestra; Alerion Biomedical Inc.) was also injected through the jugular vein. Radionuclide imaging was performed 3 h after tracer injection using a dual-head micro-SPECT γ-camera with micro-CT (X-SPECT; Gamma Medica, Inc.). Micro-SPECT images of the aorta were acquired in 64 × 64 matrix, 32 stops at 120 s per stop on 140-keV photopeak of ^{99m}Tc with 15% windows using a low-energy, high-resolution pinhole collimator. The pinhole aperture size was 1 mm. Immediately after SPECT acquisition, a micro-CT scan was acquired without having to move the animals. The micro-CT used an x-ray tube operating at 50 kVp and 0.6 mA. Images were captured for 2.5 s per view for 256 views in 360° rotation. The micro-CT images were transferred to 256 × 256 matrix and micro-CT tomographic studies were fused, allowing the achievement of simultaneous scintigraphic and anatomic information in all tomographic scans in the 3 different spatial axes. After in vivo imaging, animals were sacrificed as detailed in the histology section, and aortas were carefully harvested after perfusion fixation. Planar images of the ex vivo aorta were acquired 5 h after tracer injection for 30 min in 128 × 128 matrix using a low-energy, high-resolution, parallel-hole collimator. A time-line diagram of the experimental protocol was shown in Figure 1.

Aorta Preparation

Blood was collected by cardiac puncture at the time of death. The animals were perfused through a puncture in the left ventricle under physiologic pressure with cold phosphate-buffered saline (PBS) and then with 4% paraformaldehyde in PBS, pH 7.4. The entire length of the aorta was exposed and cleaned of adherent fat and connective tissue before removal. After cutting aortas into 3 pieces, tissue samples were fixed overnight with 4% paraformaldehyde at 4°C. Thereafter, fixed tissue was stored in PBS/0.02% sodium azide (NaN_3) at 4°C until use.

Quantitative Uptake of ^{99m}Tc-Annexin A5 in Atherosclerotic Lesions and Radiotracer Biodistribution

After ex vivo imaging, aortas were cut into 3 pieces (ascending aorta and arch, thoracic aorta, abdominal aorta). For quantitative uptake data, ^{99m}Tc uptake in the slices of the aorta was determined with γ-scintillation counting (1480 Wizard 3″; Wallac Co.) and expressed as the percentage injected dose per gram (%ID/g) aortic tissue. Similar biodistribution studies for the blood, heart, lung, spleen, and kidney were also undertaken and uptake was expressed as %ID/g.

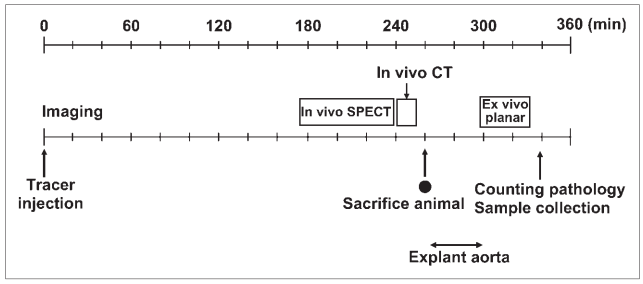

FIGURE 1. Schematic presentation of experimental protocol. Three hours after annexin A5 injection, in vivo micro-SPECT was acquired for approximately 1 h and, immediately after SPECT acquisition, in vivo micro-CT was acquired for 15 min. After the in vivo imaging study, animals were sacrificed and aortas were explanted, and ex vivo planar imaging was acquired for 30 min.

Histologic and Immunohistochemical Evaluations of Atherosclerotic Lesions

Each specimen was subdivided into 5 or 6 equidistant sections and embedded in paraffin. Serial 5-μm-thick sections were cut and mounted on adhered slides pretreated with vectabond reagent (SP-1800; Vector). Deparaffinization was performed by heating the sections for 25 min at 56°C. The tissue was then dehydrated twice using a xylene bath and a graded series of ethanol. Tissue sections were stained with hematoxylin and eosin and Movat's pentachrome stain. Histologic specimens were analyzed on the basis of the classification scheme of the American Heart Association (AHA) (*13*).

For immunohistochemical characterization of cellular components of lesions in deparaffinized tissue sections, endogenous peroxidase was blocked by treatment with 3% H_2O_2 in PBS for 5 min at room temperature. Nonspecific background staining was blocked by a 1-h incubation in 3% bovine serum albumin with 0.3% Triton X-100 at room temperature. Macrophages were detected with Mac-3 antibody (0.16 μg/mL, 550292; BD Biosciences), and smooth muscle cells (SMCs) were stained with antiactin antibody (0.25 μg/mL, MAB1420; R&D). Sections were incubated with the primary antibodies overnight at 4°C and rinsed 3 times with PBS and 0.1% Triton X-100. The sections were then incubated with biotinylated secondary antibody followed by incubation with an ABC kit reagent (Vector) for 1 h each at room temperature. Finally, after washing 3 times with PBS, the sections were incubated for approximately 2–5 min with diaminobenzidine (DAB) (Vector) for the color reaction product.

In situ cell death (apoptosis) was detected by terminal deoxyribonucleotide transferase (TDT)-mediated nick-end labeling (TUNEL) staining, using, a TACS (Trevigen) apoptosis detection kit. Deparaffinized sections were treated with 3% H_2O_2 in doubly distilled water for 5 min to inactivate endogenous peroxidase. The sections were rinsed with PBS and microwaved for 2 min in preheated 0.01 mol/L citrate buffer using a 1.2-kW microwave oven at power level 4. Then sections were digested with 20 μg/mL of proteinase K in PBS for 15 min at room temperature. Exposed DNA fragments were labeled with biotinylated nucleotides and TDT overnight at 4°C. The incorporation of biotinylated nucleotides into DNA was detected with a streptavidin-conjugated horseradish peroxidase. A positive reaction was visualized with TACS blue label. Counterstaining with nuclear fast red was performed before final analysis of apoptosis cells.

Histochemical staining was observed under an Axiovert-200 inverted microscope (Carl Zeiss) and images were acquired with a Zeiss Axiocam high-resolution digital color camera (1,300 × 1,030 pixels) using Axiovision 3.1 software. Five to 8 images were acquired for each animal. These digital images were analyzed using KS300 analysis program (Zeiss). The percentage immunostaining area (immunostaining area/total image area × 100) was determined for all of the markers studied by averaging the percentage field area of several images per section that cover most or all of the region of study. Quantitative comparisons of the percentage immunostaining area with %ID/g uptake of ^{99m}Tc-annexin A5 were performed on sections processed at the same time.

Direct Localization of Annexin A5 in ApoE$^{-/-}$ Mice

In a separate experiment of 2 chow-fed apoE$^{-/-}$ mice, annexin A5 was localized in atherosclerotic plaques by histology. Biotinylated annexin A5 (0.5 mg, Apoptest-Biotin; NeXins Research) was injected intravenously. Thirty minutes after injection, the mice were euthanized and perfusion-fixed with 4% *N*-2-hydroxyethylpiperazine-*N*-2-ethanesulfonic acid–buffered formalin. The major arteries were carefully harvested and processed for paraffin embedding.

For annexin A5–biotin staining, serial sections (4 μm) were deparaffinized in xylene and treated with 0.3% H_2O_2 for 20 min to inactivate endogenous peroxides. Arterial sections were then incubated in a streptavidin-conjugated horseradish peroxidase overnight at 4°C. Annexin A5 was visualized with the chromogenic substrate DAB after enhancement with tyramide (catalyzed signal amplification system; DAKO). The apoptotic cells in the annexin uptake regions were identified with DNA fragmentation staining. The kidney was used as a positive control, as the biodistribution of annexin A5 is highest in this organ, and positive labeling represents successfully injected animals.

Statistical Analysis

The γ-scintillation counts were calculated as %ID/g of tissues or blood, and all data are presented as mean ± SD. To determine the statistical significance of differences between groups, 1-tailed ANOVA followed by the Scheffe post hoc test for multiple comparisons was done; $P < 0.05$ was considered as statistically significant. The extent of macrophage infiltration, SMC prevalence, and apoptotic cells were calculated as the percentage field area of several images per section that covered most or all of the tissue sections stained immunohistochemically. The data are also presented as mean ± SD for all groups of animals and statistical analyses were performed as described. The correlation between the radiolabeled annexin A5 uptake and the cellular composition was calculated by linear regression analysis.

RESULTS

Noninvasive Detection of Aortic Atherosclerosis in Transgenic Mice

In vivo micro-SPECT/micro-CT with ^{99m}Tc-annexin A5 allowed noninvasive visualization of atherosclerotic lesions and the uptake was confirmed in the ex vivo imaging of the harvested aorta. The lesions were best visible in the aortic arch of apoE$^{-/-}$ and LDLR$^{-/-}$ mice (Figs. 2 and 3, respectively). The most intense uptake was found in cholesterol-fed apoE$^{-/-}$ mice and chow-fed apoE$^{-/-}$ mice. LDLR$^{-/-}$ mice receiving a normal mouse chow showed minimal lesions, but those receiving a high-cholesterol diet had lesions somewhat similar to those of normal apoE$^{-/-}$ mice (Figs. 2 and 3). No annexin A5 uptake was observed in the control animals (Figs. 2A and 3A). Calcification in the aortic arch was also seen by micro-CT, which occurred in all cholesterol-fed apoE$^{-/-}$ mice, 4 of 6 (67%) chow-fed apoE$^{-/-}$ mice, and 4 of 7 (57%) cholesterol-fed LDLR$^{-/-}$ mice (Fig. 2C).

Quantitative ^{99m}Tc-Annexin A5 Uptake

Quantitative ^{99m}Tc-annexin A5 uptake paralleled the observation on the in vivo and ex vivo imaging (Figs. 2 and 3). The maximum uptake in the atherosclerotic lesions was observed in cholesterol-fed apoE$^{-/-}$ (0.88 ± 0.27 %ID/g) mice, followed by chow-fed apoE$^{-/-}$ (0.60 ± 0.16 %ID/g) mice, cholesterol-fed LDLR$^{-/-}$ (0.59 ± 0.14 %ID/g), and

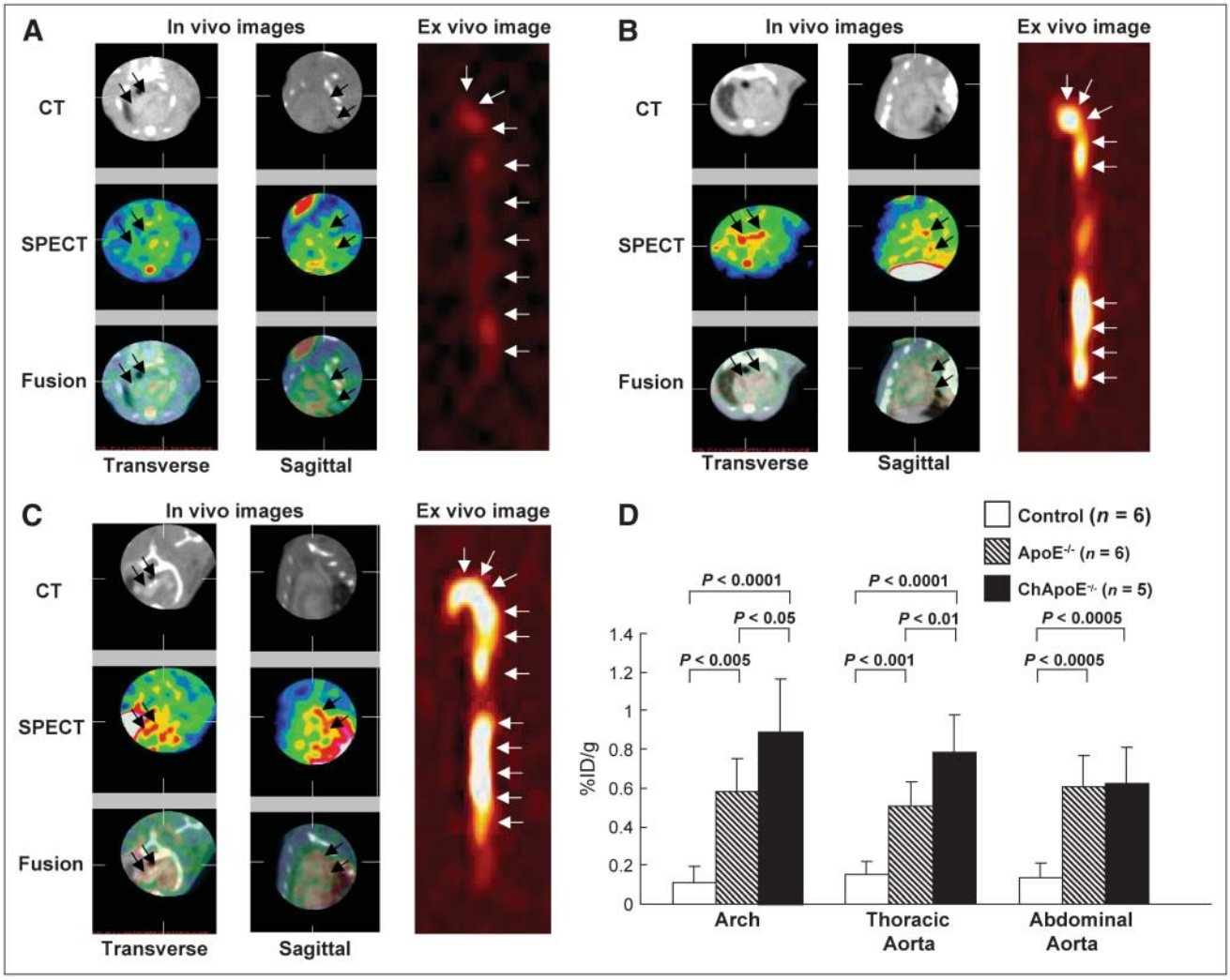

FIGURE 2. In vivo and ex vivo images of control mice (A) and apoE$^{-/-}$ mice without cholesterol diet (B) and with cholesterol diet (C). For all images, left panel represents transverse images, middle panel represents sagittal images, and right panel represents ex vivo images (A–C). Top panel shows micro-CT, middle panel shows micro-SPECT, and bottom panel shows fusion images. (A) No obvious annexin A5 uptake was seen on either in vivo or ex vivo images of control animals. (B) Distinct uptake was observed in the arch on in vivo images and in the arch and abdominal aorta on ex vivo image. (C) Distinct uptake and calcification were observed in the arch on the in vivo images; annexin uptake was seen in whole aorta on the ex vivo image. (D) Quantitative uptake was highest in cholesterol-fed apoE$^{-/-}$ mice, followed by chow-fed apoE$^{-/-}$ and control mice in lesions at arch, thoracic, or abdominal level. Ch = cholesterol fed.

chow-fed LDLR$^{-/-}$ (0.40 ± 0.13 %ID/g) mice (Figs. 2D and 3D). The maximum uptake was found in the aortic arch in cholesterol-fed apoE$^{-/-}$ mice. The uptake was higher and lesions were more prominently observed in any aortic lesion of apoE$^{-/-}$ mice compared with LDLR$^{-/-}$ mice regardless of diet type. The uptake in cholesterol-fed animals was higher than chow-fed transgenic animals. The uptake was only marginally increased in chow-fed LDLR$^{-/-}$ mice.

The highest uptake of ^{99m}Tc-annexin A5 was in the kidney (104.7 ± 20.7 %ID/g), followed by liver (8.45 ± 2.46 %ID/g), spleen (4.96 ± 2.17 %ID/g), lung (2.36 ± 1.37 %ID/g), and heart (0.69 ± 1.06 %ID/g) in all animals irrespective of diet or genetic background. The annexin A5 uptake in blood was 0.30 ± 0.03 %ID/g, 0.32 ± 0.09 %ID/g, 0.43 ± 0.06 %ID/g, 0.47 ± 0.07 %ID/g, and 0.55 ± 0.07 %ID/g in control, chow-fed LDLR$^{-/-}$, cholesterol-fed LDLR$^{-/-}$, chow-fed apoE$^{-/-}$, and cholesterol-fed apoE$^{-/-}$ mice, respectively.

Histologic Characterization of Atherosclerotic Lesions

Atherosclerotic lesions, ranging from foam cell–rich fatty streaks to fibrous plaques with large necrotic cores, were obtained. The necrotic cores comprised extracellular lipid, cholesterol clefts, and foam cells. Such plaques were typically observed in the aortic neointima of cholesterol-fed apoE$^{-/-}$, chow-fed apoE$^{-/-}$, and cholesterol-fed LDLR$^{-/-}$ mice (Fig. 4).

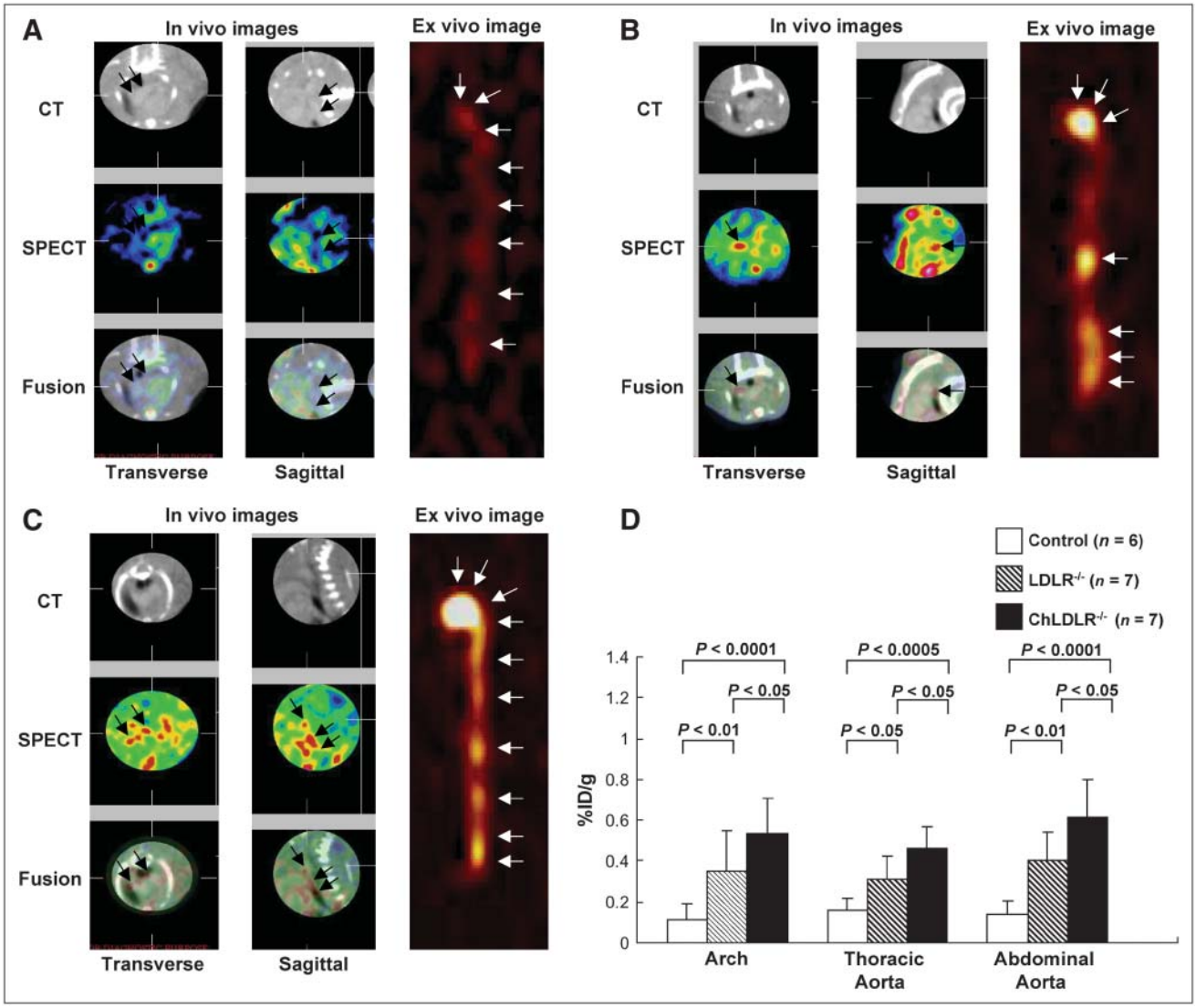

FIGURE 3. In vivo and ex vivo images in control mice (A) and LDLR$^{-/-}$ mice without cholesterol diet (B) and with cholesterol diet (C). For all images, left panel represents transverse images, middle panel represents sagittal images, and right panel represents ex vivo images (A–C). Top panel shows micro-CT, middle panel shows micro-SPECT, and bottom panel shows fusion images. (A) No obvious annexin A5 uptake was seen on either in vivo or ex vivo images of control animals. (B) Significant uptake was observed in the arch on in vivo images and in the arch and abdominal aorta on ex vivo image. (C) Distinct uptake was observed in the arch on in vivo images and distinct uptake was seen in whole aorta on ex vivo image. However, uptake in any area was lower compared with that of apoE$^{-/-}$ mice. (D) Quantitative uptake was highest in cholesterol-fed LDLR$^{-/-}$ mice, followed by chow-fed LDLR$^{-/-}$ and control mice in lesions at arch, thoracic, or abdominal level. Ch = cholesterol fed.

The atherosclerotic plaques were smallest in chow-fed LDLR$^{-/-}$ mice. In contrast, the lesion severity was significantly increased in cholesterol-fed LDLR$^{-/-}$ and apoE$^{-/-}$ mice (Fig. 4A). Lesions were not significantly different in apoE$^{-/-}$ mice with or without the cholesterol diet. Standard lesions in these animals were described as AHA types I–III, type IV, type V, and type V in chow-fed LDLR$^{-/-}$, cholesterol-fed LDLR$^{-/-}$, chow-fed apoE$^{-/-}$, and cholesterol-fed apoE$^{-/-}$ mice, respectively. The mean annexin A5 uptake was significantly higher in aortic segments with AHA type V lesion (0.72 ± 0.12 %ID/g) than type IV (0.56 ± 0.16 %ID/g, $P < 0.05$) or type III (0.35 ± 0.07 %ID/g, $P < 0.005$).

Immunohistochemical staining confirmed the lesions to be rich in macrophage-derived foam cells, in some SMCs, and in a variable extent of macrophage apoptosis (Figs. 4B–4D). Macrophage infiltration was measured by Mac-3 surface antigens (Fig. 4B). Mac-3–positive cells were seen in significantly larger number in cholesterol-fed LDLR$^{-/-}$ (0.41% ± 0.25%) mice than chow-fed LDLR$^{-/-}$ (0.068% ± 0.011%) mice ($P < 0.01$) (Fig. 5A). On the other hand, macrophage contents were only marginally different in cholesterol-fed (0.52% ± 0.32%) mice versus chow-fed apoE$^{-/-}$ (0.42% ± 0.19%) mice ($P = 0.59$) (Fig. 5A). SMCs in the plaques were detected by α-actin (Fig. 4C). SMCs prevalence was significantly lower in neointima as

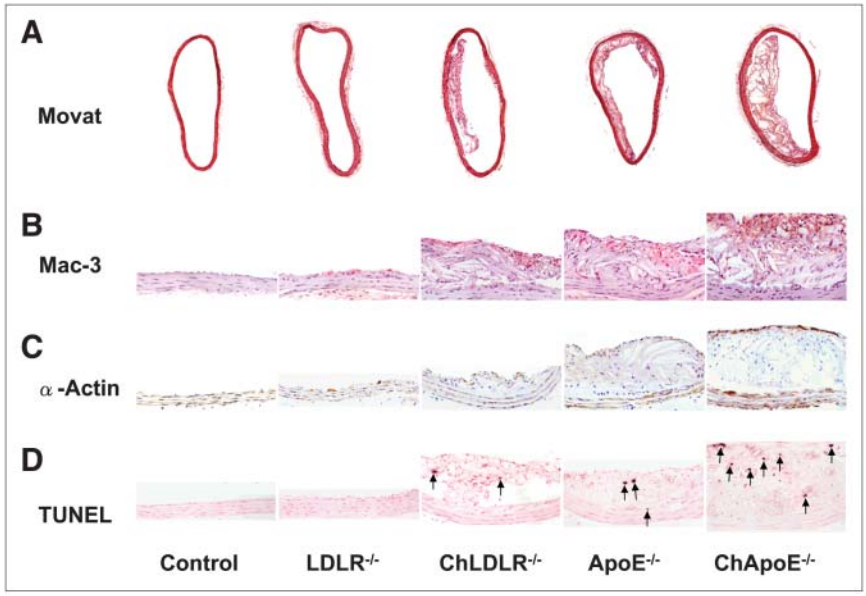

FIGURE 4. Histopathologic characterization of atherosclerotic lesions including Movat's pentachrome staining (×100) (A), Mac-3 antibody staining (×400) (B), α-actin staining (×400) (C), and TUNEL staining (×400) (D) in control, chow-fed LDLR$^{-/-}$, cholesterol-fed LDLR$^{-/-}$, chow-fed apoE$^{-/-}$, and cholesterol-fed apoE$^{-/-}$ mice. (B) Prevalence of Mac-3–positive cells was significantly higher in cholesterol- and chow-fed apoE$^{-/-}$ and cholesterol-fed LDLR$^{-/-}$ mice than that in chow-fed LDLR$^{-/-}$ mice. (C) Prevalence of SMC, detected by α-actin, was significantly lower compared with macrophages. α-Actin–positive cells were predominantly located in fibrous caps and were relatively more commonly observed in cholesterol- and chow-fed apoE$^{-/-}$ mice than in cholesterol- or chow-fed LDLR$^{-/-}$ mice. (D) TUNEL-positive nuclei in core region were more frequently observed in apoE$^{-/-}$ mice than in LDLR$^{-/-}$ mice and more so in cholesterol-fed animals (arrows). TUNEL-positive nuclei were not detected in chow-fed LDLR$^{-/-}$ mice. Ch = cholesterol fed.

compared with macrophages (Figs. 4B and 4C). No significant difference was seen in α-actin–positive cells observed in the fibrous cap of the plaques among the 4 transgenic animals (Figs. 4C and 5A). TUNEL staining was performed for the detection of apoptosis. Most apoptosis was found in the core region. The TUNEL-positive nuclei were more frequently observed in apoE$^{-/-}$ mice than in LDLR$^{-/-}$ mice, and more so in cholesterol-fed mice than in chow-fed mice (Fig. 4D).

Significant correlations were observed between the percentage field area and %ID/g of ^{99m}Tc-annexin A5. An excellent correlation of annexin uptake was evident with the percentage field area of Mac-3 antibody or TUNEL staining ($r = 0.77$, $P < 0.0001$; $r = 0.89$, $P < 0.0001$, respectively) (Figs. 5C and 5D).

Direct Localization of Annexin A5 Uptake

The target for annexin A5 in atherosclerotic lesions was identified by administration of biotinylated annexin A5 in 2 chow-fed apoE$^{-/-}$ mice (Fig. 6). Thirty minutes after administration, the bulk of circulating annexin A5–biotin (Fig. 6B) was found to localize with macrophage-rich areas

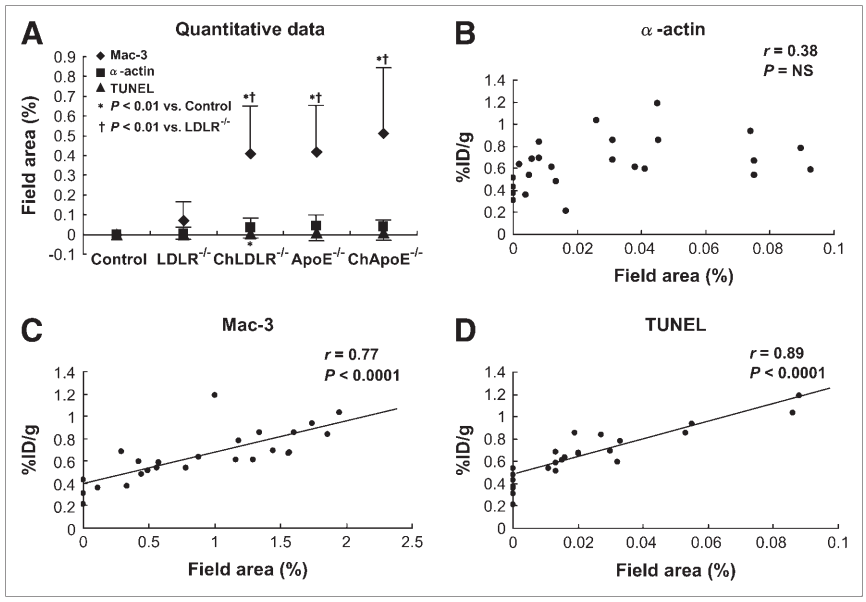

FIGURE 5. Quantitative histologic analysis and correlation with radiotracer uptake. (A) Percentage prevalence of cellular components in various groups. Percentage immunostaining field areas for macrophages are highest in cholesterol-fed apoE$^{-/-}$ mice, followed by chow-fed apoE$^{-/-}$, cholesterol-fed LDLR$^{-/-}$, and chow-fed LDLR$^{-/-}$ mice. Similar trends are seen for apoptotic nuclei. Correlation of annexin A5 uptake is evident with macrophages (C) and apoptosis (D), but no significant correlation is seen with SMCs (B). Ch = cholesterol fed.

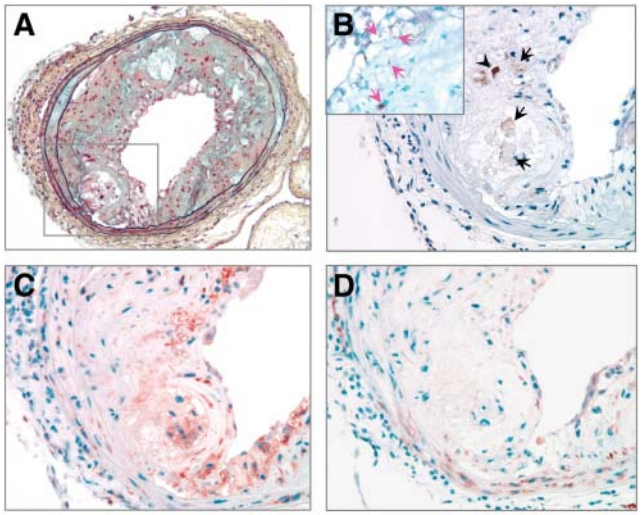

FIGURE 6. Localization of annexin A5 spontaneous atherosclerotic lesions. Biotinylated annexin A5 was injected intravenously into apoE$^{-/-}$ mice and traced histochemically in arterial wall. (A) Advanced atherosclerotic lesion in femoral artery (Movat's pentachrome, ×100). Area outlined by black box in A is magnified in B–D. (B) Annexin uptake (black arrowhead, apoptotic; black arrows, nonapoptotic) was localized in macrophages identified by Mac-3 antibody staining as shown in C (×400). Inset in B shows that some nuclei were apoptotic (black reaction product, pink arrows) and localized in same area (×1,000, blue-green nuclear counterstain; interference contrast microscopy). (D) Annexin A5 uptake was not associated with SMCs.

of the plaque in apoE$^{-/-}$ mice (Fig. 6C). A large number of cells showing annexin A5 uptake was found to be positive for apoptosis, as confirmed by the DNA fragmentation study (Fig. 6B, inset). Annexin uptake occurred in both apoptotic cells (black arrowhead) and nonapoptotic cells (black arrows) in macrophage-rich regions (Fig. 6B). Kidney sections from apoE$^{-/-}$ mice injection with annexin A5–biotin showed extensive staining in cortical regions (data not shown in Fig. 6).

DISCUSSION

The present study demonstrates the feasibility of noninvasive detection of atherosclerotic lesions with coregistered micro-CT/micro-SPECT with ^{99m}Tc-annexin A5 in different murine models of atherosclerosis. Histologic measures of macrophage content and apoptosis correlated well with ^{99m}Tc-annexin A5 uptake. These data suggest that it may be feasible to longitudinally image atherosclerosis, to ascertain its natural history through noninvasive methods, and to perform intervention experiments in mouse models of human atherosclerosis.

Target for Annexin Imaging in Atherosclerotic Mouse Model

It is well established that annexin A5 binds to apoptotic cells with nanomolar affinity (*11*). Such cells express abundant PS on the cell membrane (*10*). Because apoptosis is strongly correlated with the vulnerability of plaque to rupture (*14*), annexin A5 imaging has been considered to be a surrogate for identification of unstable atherosclerotic lesions. The cell types undergoing apoptosis in the vessel wall are endothelial cells (*15*), vascular SMCs (*16*), inflammatory cells such as macrophages (*14,17*), and adventitial fibrosis (*18*). Apoptosis in vulnerable plaques is localized to inflammatory cells in the fibrous cap, deep intima, and shoulder regions; a fair degree of apoptosis is also found in macrophages surrounding the lipid core (*17*). It has been proposed that macrophage cell death may promote plaque instability by contributing to the size of the necrotic core (*17*). On the other hand, apoptosis of vascular SMCs within the fibrous cap may represent a chronic process leading to fibrous cap thinning (*19*). Extensive apoptosis of macrophages at the site of plaque rupture has been suggested to play a role in acute coronary events (*14*).

Noninvasive recognition of apoptotic cells has become possible by targeting of abnormal expression of PS on the cell membrane with the help of annexin A5. In previous rabbit and human studies, the binding of radiolabeled annexin A5 was increased in areas of atherosclerotic plaque and was predominantly localized to macrophages (*9,20*). These results are in concordance with our observation in apoE$^{-/-}$ and LDLR$^{-/-}$ mice. However, in the present study, radiolabeled tracer uptake was also seen in nonapoptotic macrophages. As inflammation constitutes the most important substrate for plaque vulnerability, annexin A5 imaging should be of immense value in the detection of unstable lesions. In clinical scenarios, PS is also expressed by crenating red blood cells in the regions of intraplaque hemorrhage that have also been proposed as the harbinger of plaque rupture (*21*). Therefore, molecular nuclear imaging may allow targeting of pathophysiologic process within the plaque critical to lesion instability.

Rosenfeld et al. reported that atherosclerotic lesions are distributed throughout the arterial tree of apoE$^{-/-}$ mice between ages of 24 and 60 wk (*22*). The innominate artery exhibits a highly consistent rate of lesion progression and develops vascular narrowing characterized by atrophic media and perivascular inflammation. The hyperlipidemic animals particularly demonstrate characteristics of advanced lesions in the innominate artery (*22*). Our results revealing maximal annexin A5 uptake in the aortic arch support the results of Rosenfeld et al. However, we used slightly older mice (mean age, 62 ± 0.9 wk old).

In a previous study using radiolabeled oxidation-specific antibody (oxidation-specific antibody to malondialdehyde-LDL [MDA2]) in LDLR$^{-/-}$ mice, enhanced ^{125}I-MDA2 uptake correlated well with increased oxidized LDL (OxLDL) and macrophage immunostaining, suggesting plaque instability (*23*). In mice for which the high fat/cholesterol diet was withdrawn and replaced with normal mouse chow or chow supplemented with antioxidants, there was significant reduction in the ^{125}I-MDA2 uptake, which was correlated with significant reduction in the macrophage content and OxLDL, detected by immunostaining with

several murine and human OxLDL antibodies. Interestingly, in these areas of reduced ^{125}I-MDA2 uptake, there was also increased SMC and collagen content, suggesting that the uptake of ^{125}I-MDA2 reflected the development of plaque stabilization. This finding suggests that noninvasive imaging approaches may ultimately quantify and detect the presence of plaque stability or instability. Our results in the present study, which demonstrated that increased ^{99m}Tc-annexin A5 uptake was seen in plaques rich in macrophages and with a paucity of SMCs, are in accord with the previous results. Future studies can now be designed to longitudinally assess the regression of atherosclerosis in the same group of animals with noninvasive imaging models, such as with annexin A5.

Difference in ^{99m}Tc-Annexin A5 Uptake in ApoE$^{-/-}$ and LDLR$^{-/-}$ Mice With or Without Cholesterol Diet

In our results, the %ID/g ^{99m}Tc-annexin A5 uptake was higher in apoE$^{-/-}$ mice than in LDLR$^{-/-}$ mice regardless of diet. An earlier study had reported that the apoE$^{-/-}$ mice on a normal chow diet had much more profound hypercholesterolemia compared with the LDLR$^{-/-}$ mice (*24*). In addition, the animals exhibit quantitative and qualitative differences in plasma cholesterol levels. In the apoE$^{-/-}$ mice, cholesterol accumulated primarily in large lipoprotein particles, primarily in intermediate-density lipoproteins, but also in very-low-density lipoproteins and chylomicron remnants (*1,2*). In contrast, the LDLR$^{-/-}$ mice had a much more selective elevation in LDL (*3,8*). We did not measure the plasma levels of cholesterol in this study.

In the present study, the %ID/g ^{99m}Tc-annexin uptake was higher in cholesterol-fed transgenic mice compared with chow-fed mice. As previously reported, an abundant cell-poor, lipid-rich core developed in the atherosclerotic lesions of cholesterol-fed animals (*25*). The core was characterized by extracellular lipid deposition, cholesterol crystal, and cell death and was situated in the deep layer of the plaque. In experimental studies using hyperlipidemic mice, apoptosis was also observed in the advanced vascular lesions of APOE*3-Leiden transgenic mice (*26*) and the aortas of hyperlipidemic apoE$^{-/-}$- and LDLR$^{-/-}$-deficient mice (*27*). Apoptosis was involved in the active turnover of foam cells of both macrophage and SMC lineage, even in the early atherosclerotic lesions of transgenic mice. However, the effects of additional cholesterol on atherosclerotic lesions remain to be investigated. Our results, which demonstrated that additional cholesterol diet for hyperlipidemic transgenic mice increases the presence and extent of apoptosis, may provide an important standpoint with regard to plaque stabilization rather than plaque regression for advanced atherosclerotic lesions.

CONCLUSION

Our study demonstrates the feasibility of noninvasive detection of the presence and extent of atherosclerosis in transgenic mice with radiolabeled annexin A5. This imaging approach in these mouse models will allow opportunities to noninvasively characterize the pathogenesis of atherosclerosis and the impact of therapeutic interventions.

ACKNOWLEDGMENTS

This study was supported by National Institutes of Health grant 1 RO1 HL 68657-01 and in part by the Donald W. Reynolds Foundation, Las Vegas, NV.

REFERENCES

1. Plump AS, Smith JD, Hayek T, et al. Severe hypercholesterolemia and atherosclerosis in apolipoprotein E-deficient mice created by homologous recombination in ES cells. *Cell.* 1992;71:343–353.
2. Zhang SH, Reddick RL, Piedrahita JA, Maeda N. Spontaneous hypercholesterolemia and arterial lesions in mice lacking apolipoprotein E. *Science.* 1992;258:468–471.
3. Ishibashi S, Brown MS, Goldstein JL, Gerard RD, Hammer RE, Herz J. Hypercholesterolemia in low density lipoprotein receptor knockout mice and its reversal by adenovirus-mediated gene delivery. *J Clin Invest.* 1993;92:883–893.
4. Jawien J, Nastalek P, Korbut R. Mouse models of experimental atherosclerosis. *J Physiol Pharmacol.* 2004;55:503–517.
5. Nakashima Y, Plump AS, Raines EW, Breslow JL, Ross R. ApoE-deficient mice develop lesions of all phases of atherosclerosis throughout the arterial tree. *Arterioscler Thromb.* 1994;14:133–140.
6. Reddick RL, Zhang SH, Maeda N. Atherosclerosis in mice lacking apo E: evaluation of lesional development and progression. *Arterioscler Thromb.* 1994;14:141–147.
7. Palinski W, Ord VA, Plump AS, Breslow JL, Steinberg D, Witztum JL. ApoE-deficient mice are a model of lipoprotein oxidation in atherogenesis: demonstration of oxidation-specific epitopes in lesions and high titers of autoantibodies to malondialdehyde-lysine in serum. *Arterioscler Thromb.* 1994;14:605–616.
8. Ishibashi S, Goldstein JL, Brown MS, Herz J, Burns DK. Massive xanthomatosis and atherosclerosis in cholesterol-fed low density lipoprotein receptor-negative mice. *J Clin Invest.* 1994;93:1885–1893.
9. Kolodgie FD, Petrov A, Virmani R, et al. Targeting of apoptotic macrophages and experimental atheroma with radiolabeled annexin V: a technique with potential for noninvasive imaging of vulnerable plaque. *Circulation.* 2003; 108:3134–3139.
10. Kietselaer BL, Reutelingsperger CP, Heidendal GA, et al. Noninvasive detection of plaque instability with use of radiolabeled annexin A5 in patients with carotid-artery atherosclerosis. *N Engl J Med.* 2004;350:1472–1473.
11. Fadok VA, Voelker DR, Campbell PA, Cohen JJ, Bratton DL, Henson PM. Exposure of phosphatidylserine on the surface of apoptotic lymphocytes triggers specific recognition and removal by macrophages. *J Immunol.* 1992;148:2207–2216.
12. Dachary-Prigent J, Freyssinet JM, Pasquet JM, Carron JC, Nurden AT. Annexin V as a probe of aminophospholipid exposure and platelet membrane vesiculation: a flow cytometry study showing a role for free sulfhydryl groups. *Blood.* 1993;81:2554–2565.
13. Stary HC, Chandler AB, Dinsmore RE, et al. A definition of advanced types of atherosclerotic lesions and a histological classification of atherosclerosis: a report from the Committee on Vascular Lesions of the Council on Arteriosclerosis, American Heart Association. *Arterioscler Thromb Vasc Biol.* 1995;15: 1512–1531.
14. Kolodgie FD, Narula J, Burke AP, et al. Localization of apoptotic macrophages at the site of plaque rupture in sudden coronary death. *Am J Pathol.* 2000;157: 1259–1268.
15. Tricot O, Mallat Z, Heymes C, Belmin J, Leseche G, Tedgui A. Relation between endothelial cell apoptosis and blood flow direction in human atherosclerotic plaques. *Circulation.* 2000;101:2450–2453.
16. Walsh K, Smith RC, Kim HS. Vascular cell apoptosis in remodeling, restenosis, and plaque rupture. *Circ Res.* 2000;87:184–188.
17. Bjorkerud S, Bjorkerud B. Apoptosis is abundant in human atherosclerotic lesions, especially in inflammatory cells (macrophages and T cells), and may contribute to the accumulation of gruel and plaque instability. *Am J Pathol.* 1996;149:367–380.

18. Bjorkerud B, Bjorkerud S. Contrary effects of lightly and strongly oxidized LDL with potent promotion of growth versus apoptosis on arterial smooth muscle cells, macrophages, and fibroblasts. *Arterioscler Thromb Vasc Biol.* 1996;16: 416–424.
19. Geng YJ, Henderson LE, Levesque EB, Muszynski M, Libby P. Fas is expressed in human atherosclerotic intima and promotes apoptosis of cytokine-primed human vascular smooth muscle cells. *Arterioscler Thromb Vasc Biol.* 1997;17: 2200–2208.
20. Narula J, Hofstra L. Imaging myocardial necrosis and apoptosis. In: Dilsizian V, Narula J, eds. *Atlas of Nuclear Cardiology.* Philadelphia, PA: Current Medicine; 2003:197-216.
21. Kolodgie FD, Gold HK, Burke AP, et al. Intraplaque hemorrhage and progression of coronary atheroma. *N Engl J Med.* 2003;349:2316–2325.
22. Rosenfeld ME, Polinsky P, Virmani R, Kauser K, Rubanyi G, Schwartz SM. Advanced atherosclerotic lesions in the innominate artery of the ApoE knockout mouse. *Arterioscler Thromb Vasc Biol.* 2000;20:2587–2592.
23. Torzewski M, Shaw PX, Han KR, et al. Reduced in vivo aortic uptake of radiolabeled oxidation-specific antibodies reflects changes in plaque composition consistent with plaque stabilization. *Arterioscler Thromb Vasc Biol.* 2004;24: 2307–2312.
24. Ishibashi S, Herz J, Maeda N, Goldstein JL, Brown MS. The two-receptor model of lipoprotein clearance: tests of the hypothesis in "knockout" mice lacking the low density lipoprotein receptor, apolipoprotein E, or both proteins. *Proc Natl Acad Sci U S A.* 1994;91:4431–4435.
25. Kockx MM, De Meyer GR, Muhring J, Bult H, Bultinck J, Herman AG. Distribution of cell replication and apoptosis in atherosclerotic plaques of cholesterol-fed rabbits. *Atherosclerosis.* 1996;120:115–124.
26. Lutgens E, Daemen M, Kockx M, et al. Atherosclerosis in APOE*3-Leiden transgenic mice: from proliferative to atheromatous stage. *Circulation.* 1999;99: 276–283.
27. Harada K, Chen Z, Ishibashi S, et al. Apoptotic cell death in atherosclerotic plaques of hyperlipidemic knockout mice. *Atherosclerosis.* 1997;135:235–239.